Multi-point LIBS measurement and kinetics modeling of sodium release from a burning Zhundong coal particle

Yingzu Liu[1,2], Yong He[1], Zhihua Wang*[,1], Kaidi Wan[1], Jun Xia[2], Jianzhong Liu[1], Kefa Cen[1]

1 State Key Laboratory of Clean Energy Utilization, Zhejiang University, 310027, Hangzhou, P.R. China

2 Department of Mechanical, Aerospace and Civil Engineering & Institute of Energy Futures, Brunel University London, Uxbridge UB8 3PH, UK

** Corresponding author: Zhihua Wang ,Tel: +86-571-87953162, Fax: +86-571-87951616, Email: wangzh@zju.edu.cn*

Abstract

A multi-point Laser-Induced Breakdown Spectroscopy (LIBS) method for quantitative measurement of sodium concentrations in the gas phase, the surface temperature and the particle diameter during the combustion of a Zhundong coal particle is presented. To obtain multi-point LIBS data, the laser focusing and signal collection optics are mounted on a translational platform which is able to traverse cyclically. With this setup multi-point LIBS measurements above a burning particle can be performed and the time-resolved sodium release process can be obtained. The results show that 42.2 % of the total sodium mass is released during the burning of the Zhundong coal sample. For a 4 mm particle, in the char burnout stage sodium is released most strongly, i.e., 87% of the total released sodium mass, while in the de-volatilization and ash reaction stages the percentages are 5% and 8%, respectively. The atomic sodium and NaOH are the most favored species at chemical equilibrium in the plume according to CHEMKIN. The sodium release is found to be closely related to the particle burning stages by analyzing the sodium release, particle surface temperature and its diameter. A linear relationship is found between the residual sodium mass in the particle and the volume of the particle. The volatile sodium release rate obeys a two-step Arrhenius expression. Predictions by the developed two-step kinetics model agree well with the measured sodium release profiles in all the three coal-burning stages.

Keywords: multi-point LIBS; Zhundong coal; sodium release; model; kinetics.

1 Introduction

The release of alkali metals is known to cause fouling and corrosion of heat transfer surfaces within boilers during combustion utilization of biomass or low-rank coal [1, 2]. During combustion, the volatile sodium will evaporate and form an initial sticky deposit on the convective heat exchange surfaces. By reacting with chloride or sulfur components in the gas phase, the sticky deposit can cause severe damage to the surfaces [3]. Furthermore, utilization of the Zhundong coal, which is believed to be one of the most abundant coalmine reserves in China, is prohibited due to its high concentration of sodium compounds [4]. Therefore, investigating the sodium reacting dynamics during coal combustion is essential to help practical utilization of high-impurity solid fuels like Zhundong coal.

Over the past decades, there have been several studies aiming to understand the release of alkali metals through offline and online measurements. The offline methods are usually based on physical and chemical analysis of fuel and ash [5-7]. According to offline results [7, 8], sodium in low-rank coal can appear in three forms: (1) water-soluble sodium which is the sodium salt and can dissolve in water; (2) organic-bounded sodium which contains the sodium bounded to organic carbon structures in the fuel; (3) insoluble sodium that has been attached to clay minerals. The first two forms of sodium compounds are releasable during coal combustion and the last one will remain in the residue ash [9]. However, the offline measurements cannot provide information about time-resolved sodium release and sodium species in the gas phase. Therefore, online methods of sodium measurement have become more popular recently. Monkhouse [10] have reviewed both online optical diagnostic methods and mass spectrometry methods of alkali species measurement in the gas phase. All these methods are helpful to understand the different forms of

sodium during its dynamic release process. In order to achieve time-resolved measurement of sodium released in the gas phase, several laser diagnostics methods have been employed in previous research, including: Laser-Induced Fragmentation Fluorescence (ELIF) [11], Tunable Diode Laser Absorption Spectroscopy (TDLAS) [12], Laser-Induced Breakdown Spectroscopy (LIBS) [13], Planar Laser-Induced Fluorescence (PLIF) [14], etc. Based on time-resolved atomic sodium results, van Eyk et al. [14, 15] used a chemical equilibrium calculation to determine the amount of volatile sodium that is releasable during coal combustion. Their results showed that nearly 90% of sodium in the coal was released. In summary, most of the abovementioned research conducted the measurement of one sodium species, i.e., atomic sodium. To the best of our knowledge, direct time-resolved measurement of the total volatile sodium flux due to a single burning particle has not been reported.

Based on online and offline measurement results, mechanisms and kinetics of alkali metal release during coal combustion and gasification have been reported. Most of the literatures pointed out that the release of alkali metals follows an Arrhenius expression [16-20]. According to the forms of alkali metals in solid fuels, the release of different classes of alkali has different reaction pathways. Water-soluble sodium is usually found to be released by evaporation and the corresponding saturation pressure has been determined by Tomeczek et al. [21]. Besides, part of water-soluble sodium can react with carboxylic acid groups, forming organic sodium like -COONa and -CNa [22, 23]. Organic sodium will be oxidized by O_2 during combustion, forming volatile sodium in the gas phase [24-26]. Moreover, insoluble sodium can react with water vapor, which also contributes to the release of sodium [15]. van Eyk et al. [17] has developed a char burnout and sodium release model based on a chemical equilibrium prediction. To the best of the

78 authors' knowledge, however, the kinetics of sodium release has not yet been directly determined
79 from measurement results. Moreover, the mechanism and kinetics of sodium release at the initial
80 coal-burning stage (the devolatilization stage) are still unknown.

81 In our previous studies, a single-point LIBS method was employed [9, 13]. In those cases, we
82 were able to get the volatile sodium concentration at only one location in each measurement. To
83 lift the limitation, the laser focusing and signal collection optics in the LIBS system were mounted
84 on a translational platform which was traversed cyclically as the particle burns in the present study.
85 Using this setup it became possible to conduct LIBS measurements at multiple points above a
86 burning particle for each case, and the time-resolved volatile sodium release process can be
87 determined. In addition, the particle surface temperature and the particle diameter were also
88 measured during sodium release measurements. The relationship between the release of volatile
89 sodium and the burning status of a particle can then be obtained. Moreover, the kinetics of volatile
90 sodium release will also be determined in this study. In the present study, coal particle size and
91 burnout time have on the same order of magnitude as in a typical CFB boiler, so this work will
92 directly impact on Zhundong-coal utilization in CFBs. Moreover, the findings of this study,
93 together with our previous work, will be important references for sodium kinetics measurement
94 and modeling of a burning coal particle in both PF and FB fields.

95 **2 Experiment setup and theory**

96 **2.1 Multi-point LIBS measurement system**

97 The LIBS method was employed to measure sodium and potassium concentrations at a single
98 point above a burning coal particle in our previous work. The design and principle of the LIBS
99 method and the details about the burner can be found in Ref. [9, 27]. In this study, a spherical

100 particle was suspended by two ceramic rods (d = 1 mm) at 10 mm above the burner plate. The
101 burner was operated with a premixed methane/air flame at an equivalence ratio of 0.8 with 0.59
102 SL/min methane and 7.06 SL/min air. The gas composition was: 3.9% O_2, 7.6% CO_2, 15.4% H_2O
103 and 72.8% N_2. The plume temperature was estimated to be ~1892 K based on CHEMKIN
104 calculations.

105 The configuration of the measurement system in this study is shown in Fig. 1a. The Nd:YAG
106 laser, which operated on the fundamental wavelength (1064 nm), was focused on a zone which is
107 10 mm above the fuel particle. A USB4000 spectrometer was adopted to collect the LIBS signal.
108 In order to generate multi-point LIBS data, the laser-focusing lens, signal collection optics and
109 spectrum detector were mounted on an electric translational platform, which was able to move
110 cyclically. In this case, the measurement point can be moved horizontally at a given height (Fig.
111 1b). The sequence timing of the laser, spectrometer and electric translational platform were
112 arranged by a digital delay/pulse generator (Model: DG535) to ensure synchrony. In the present
113 study, the laser and spectrometer were operated at 10 Hz in frequency. The motion frequency of
114 the platform was also 10 Hz and the distance of each motion is 3 mm. To be more specific, the
115 radial distances (r) of the measurement points from the centerline are: -12 mm, -9 mm, -6 mm, -3
116 mm, 0 mm (centerline), 3 mm, 6 mm, 9 mm and 12 mm, respectively. The frequency for
117 measuring the same point was 1 Hz.

118 In order to achieve quantitative measurements of sodium concentrations in the gas phase, the
119 LIBS system was calibrated by the method outlined in [9]. In the calibration experiments, an
120 ultrasonic vaporizer was used to generate a fog of sodium chloride (NaCl) solution, which was
121 carried by the feeding gas into the pilot flame through the vapor chamber. The average seeding

rate of NaCl solution was 0.69 g/min, which was calculated based on the mass loss from the seeding solution. After the correction process of self-absorption (the self-absorption by the sodium atoms in the region of the plasma and the self-absorption by sodium atoms in the calibration flame) effect [28], a linear relationship was obtained between the LIBS intensity and the concentration of Na element. In this study, since the measurement point is not far away from the centerline, the gas phase sodium in the calibration flame can be regarded as uniform. So, the relationship between the LIBS signal and the sodium concentration at each measurement point can be written as:

$$I_{LIBS,Na} = 2430 \times C_{Na},\ R^2 = 0.96 \quad (1)$$

where $I_{LIBS,Na}$ (no unit) is the intensity of sodium signals in LIBS, and C_{Na} (mg/m^3) is the sodium concentration measured at a given point, and R^2 is the coefficient of determination.

2.2 Mathematical method to determine the total mass of released sodium

By measuring sodium concentrations at all the measurement points, the release of total sodium can be determined by mathematical calculation [15]. The flux of sodium ($Na_{flux,t}$) passing through a given height at a given time can be determined from the experimental data. On the other hand, the sodium flux at any given height at a given time has the same value as the sodium release rate from the burning particle surface, which can be described as:

$$Na_{flux,t} = \int_0^{2\pi} \int_0^{\infty} u \times C_{Na} \times r \times dr \times d\theta \quad (2)$$

where u is the axial velocity, r is the radial distance from the centerline, and θ is the radian. In our experiments, the burner provided a uniform gas flow in θ direction and the particle is spherical, so Eq. (2) can be deduced as:

$$Na_{flux,t} = 2\pi \times \int_0^{\infty} u \times C_{Na} \times r \times dr \quad (3)$$

In order to simplify the calculation, we assumed the distributions of u and C_{Na} were both a

function of r, then $Na_{flux,t}$ at a given time can be approximated as follows:

$$u = f_u(r) \tag{4}$$

$$C_{Na} = f_{Na,t}(r) \tag{5}$$

$$Na_{flux,t} = 2\pi \times \int_0^{\infty} f_t(r) \times dr \tag{6}$$

At this point, $Na_{flux,t}$ at different time can be obtained from the integration of a function of r. Moreover, integrating the sodium flux with time, we can get the total mass of sodium released during a certain time period. Therefore, the integration of the sodium flux with the whole combustion duration can provide the total mass of volatile sodium in the gas phase.

$$Na_{volatile} = \int_0^{\infty} Na_{flux,t} \times dt \tag{7}$$

2.3 Particle temperature and diameter measurement

During the combustion of a coal particle, its surface emissivity will change as the main component of the particle changes from char to ash [29]. A two-color ratio pyrometer has been used to measure the variation of surface temperature of the coal particle during the whole burning period [30]. According to Yan et al. [31], the output of the two-color ratio pyrometer method's image, $I_{(\lambda,T)}$, can be proportional to the exitance of the measured surface:

$$I_{(\lambda,T)} = R_c \times S_\lambda \times \varepsilon_\lambda \times \frac{C_1}{\lambda^5} \times e^{-C_2/(\lambda T)} \tag{8}$$

where R_c is the instrument constant [32], S_λ is the spectral sensitivity of the charge coupled device (CCD) system, ε_λ is the monochromatic emissivity, T is the surface temperature, C_1 and C_2 are the first and second Planck's constants, respectively. Hence, the surface temperature can be determined by rearranging the ratio of $I_{(\lambda,T)}$ at two different wavelengths [31]:

$$T = \frac{C_2\left(\frac{1}{\lambda_2}-\frac{1}{\lambda_1}\right)}{\ln\frac{I_{\lambda_1}}{I_{\lambda_2}}+\ln\frac{S_{\lambda_1}}{S_{\lambda_2}}+\ln\frac{\varepsilon_{\lambda_1}}{\varepsilon_{\lambda_2}}+\ln\frac{\lambda_1^5}{\lambda_2^5}} \quad (9)$$

Usually, the value of $S_{\lambda 1}/S_{\lambda 2}$ in this measurement can be known from the spectral response performance of a CCD. But in our study, it was calibrated by a thermocouple in the flame in order to correct the spectral response of both the CCD and filters.

In our study, the value of $I_{(\lambda, T)}$ was collected with an intensified charge coupled device (ICCD, Model: PI MAX 3, Princeton Instrument, 1024 × 1024 pixel array). A bi-optic lens attachment (Model: LAVISION VZ-image doubler) was employed to record 2-D images of the coal particle at different wavelengths simultaneously. The images of the coal particle were collected at 1 Hz with a gate width of 800 ms throughout the whole combustion period of the coal particle. Two filters (1 nm bandwidth) centered at 633 nm and 647 nm were chosen for the two-color pyrometry technique. Moreover, since the two wavelengths are very close to each other, the differences between the corresponding spectral emissivities are neglected, i.e., $\varepsilon_{\lambda 1}/\varepsilon_{\lambda 2} \approx 1$. In addition, the variation of the diameter (d) of the burning particle can be determined from the images of thermal irradiation [33].

2.4 Coal samples

The Zhundong coal used in this study originates from Xinjiang Province, China. The Zhundong coal field contains coal reserves in the amount of 164 Gt, and it is one of the largest coal-producing areas around the world [34]. Coal particles in two different diameters (4 mm and 6 mm) were prepared in our study. First, the raw coal samples were crushed and sieved to select sub 75 μm coal particles. Then approximately 50 mg of the coal powder was pressed into a 4-mm spherical particle for measurements. To make a 6-mm spherical particle, 169 mg of the coal

176 powder was used to make sure it has the same density as with the 4 mm particle. The physical and
177 chemical analyses of the Zhundong coal are shown in Table 1. The proximate analyses were
178 determined according to the Chinese National Standard GB/T 212-2008, and the ultimate analyses
179 were determined according to the Chinese National Standard GB/T 476-2008 (carbon and
180 hydrogen), GB/T 19227-2008 (nitrogen), and GB/T 214-2007 (sulfur). In order to measure the
181 chlorine concentration, the coal sample was digested in strong acid, and then the solution was
182 measured by inductively coupled plasmas atomic emission spectroscopy (ICP-AES, Model:
183 Thermo Scientific iCAP 6300) to determine the amount of Cl.

184 The offline analysis of the sodium compounds of Zhundong coal was shown in Table 2. The
185 ash was prepared in a muffle furnace at 1000 °C in accordance with the Chinese National Standard
186 GB/T 1574-2007. The mass fractions of different classes of Na compounds in Zhundong coal and
187 ash were determined by the sequential extraction method [8, 9]. The different sodium compounds
188 were distinguished based on their solubility by stepwise extraction using water, 1 mol/L
189 ammonium acetate and 1 mol/L hydrochloric acid. The detailed sequential extraction procedure
190 can be found in our previous work [35]. As the results showed, the water-soluble sodium
191 contributes dominantly to the sodium released in the gas phase. The relative released proportion,
192 which is defined as the ratio of the sodium mass remaining in ash to that in the raw coal particle
193 sample for a specific sodium class, is the highest for NH_4Ac-soluble sodium. In the offline
194 chemical measurement, about 47.5% of sodium was found to have released during the combustion
195 process.

196 **3 Results and discussion**

197 **3.1 Multi-point LIBS measurement**

198 The distribution of sodium concentrations along the radial direction at a given height above
199 the coal particle can be used for calculating the mass of sodium released in the gas phase for a
200 burning particle, as discussed in section 2.2. The measurement results at 10 mm above a burning
201 4-mm particle is shown in Fig. 2. Each measurement has been repeated three times and the result
202 shows their average. The sodium concentration profiles at different points have the same shape as
203 those in our previous work [13, 36]. Each of them can be clearly divided into three stages (the
204 de-volatilization stage, the char burnout stage and the ash reaction stage) by two peaks. As r
205 becomes larger, the sodium concentration decreases. Moreover, the peak magnitude and duration,
206 in which sodium can be detected, of the curve decrease as the distance of the measurement point
207 from the centerline increases. The longest duration is about 1200 s for the measurement point on
208 the centerline, which suggests the integration time period for the sodium flux calculation.
209 Considering the sodium concentration at r = 15 mm is too low to be detected, the radial distance
210 for integration was taken from r = 0 to 15 mm.

211 In section 2.2, we developed a method for predicting the mass of sodium released in the gas
212 phase. In order to verify the assumptions made in Eq. (5), specific LIBS results chosen from the
213 three different stages during the combustion of a 4-mm particle are shown in Fig. 3a. The
214 relationship between the sodium concentration and the radial distance at a given time is fitted to a
215 2nd-order polynomial:

$$f_{na,t}(r) = a_2 \times r^2 + a_1 \times r + a_0 \tag{10}$$

216 where a_2, a_1 and a_0 are the fitting coefficients and their values are shown in Table 3. By using a
217 2nd-order polynomial equation to fit the sodium concentration distribution along the radial
218 direction, the coefficient of determination R-squared (R^2) is bigger than 0.98 for all the

measurement results. For the assumption of Eq. (4), we performed a 3-D steady-type simulation using ANSYS FLUENT to investigate the velocity distribution in the gas phase when burning a 4-mm Zhundong coal particle. The Reynolds number in this study was 3.84, so the laminar module is used. The other parameters were carefully chosen to approximate the experimental conditions. A second-order upwind method was used for spatial discretization. The profile of the axial velocity at 10 mm above the particle is shown in Fig. 3b, which implies a wake flow forming downstream of the suspended coal particle, with the highest axial velocity found near r = 7.5 mm. The relationship between the axial velocity and the radial distance is fitted by a fourth-order polynomial:

$$f_u(r) = b_4 \times r^4 + b_3 \times r^3 + b_2 \times r^2 + b_1 \times r + b_0 \tag{11}$$

where b_4, b_3, b_2, b_1 and b_0 are the fitting coefficients. Their values are shown in Table 3. Since the flow rate is almost constant and the effects of shrinking of the particle on the flow field are minor, Eq. (11) will be used for the whole sodium-release period.

The aforementioned conclusions can simplify Eq. (6) so that we can perform the integration as follows:

$$Na_{flux,t} = \left[F_t(r) \right]_{0mm}^{15mm} \tag{12}$$

where $F_t(r)$ is the integral of $f_t(r)$. The results are shown in Fig. 5a and the profile in the initial stage has been zoomed in. The curve of the sodium flux is very similar to the sodium concentration profiles and we determined the three different stages shown in the Fig. 4 by the followed steps: (1) Fit our experimental results (the red line) by matlab cftool. We can then separate the first and second peaks by the trough (the first green square). Its corresponding time is what we used to define the end of the devolatilization stage; (2) Use linear fitting for the rapidly

239 decreasing stage following the second peak and the asymptotic (last) stage of our experimetal
240 results (see the two blue lines). The intersection point (the second green square) of these two
241 fitting lines is the time instant with which we separate the char burnout and ash reaction stages. In
242 this case, the three stages can be defined as: (I) de-volatilization stage: the first peak, 0 - 53 s; (II)
243 char burnout stage, 54 - 489 s; (III) ash reaction stage, 490 - 1200 s. By integrating the sodium
244 flux with time, we can get the mass of sodium released at different burning stages of the 4-mm
245 particle, as shown in Fig. 5b. The total mass of sodium released into the gas phase is 0.156
246 mg/1g-coal-particle. The total sodium element mass in the raw coal particle and in the residue ash
247 from the LIBS experiment are 0.37 mg/particle and 0.186 mg/particle, respectively, which are
248 determined using ICP-AES. From the mass balance of the sodium element, it can be deduced that
249 the proportion of the released sodium is 49.7%. The online LIBS result of the proportion of the
250 released sodium (42.2%) agrees well with both the offline chemical analysis in Table 2 (47.5%)
251 and the mass balance of sodium (49.7%). The error between these two values can be caused by
252 calibration methods, chemical methods, mathematical assumptions, etc. Furthermore, the
253 integration of the sodium flux in different stages can provide the sodium-release information
254 during the three combustion stages. The most favored sodium compound is the water-soluble
255 sodium according to Table 2. However, the release of water soluble Na is limited during
256 devolatilization stage. During the combustion process, water-soluble sodium will [17]: (I)
257 evaporate and become sodium vapor in the gas phase due to high temperature; (II) react with the
258 coal compounds like –COOH to form organic sodium and then be oxidized to form NaO or NaOH,
259 both of which will be very difficult to be released into the gas phase and will remain in the
260 residual till the end of combustion. Moreover, the duration of the devolatilization process is

usually very short, so there will still exist a significant proportion of water soluble sodium to be released in the char burnout stage. This was observed in our previous study [9]. In the char burnout stage, sodium release is the strongest. Almost 87% of the releasable sodium was released in this stage. Meanwhile, the burning of organic components not only releases organic sodium but also generates high temperatures, thus favoring the evaporation of water-soluble sodium [9]. The heterogeneous reaction between Na_2O retained in the ash and H_2O from the gas phase resulted in sodium release in a long tail period, i.e., the 'ash reaction stage' [14, 33]. However, the sodium released both in the de-volatilization stage (5%) and the ash reaction stage (8%) is very little compared with that in the char burnout stage.

In our recent work [37], we have used the PLIF method to measure the release of atomic sodium. Based on the integration results of sodium flux in the three different stages from the PLIF (atomic sodium) and multi-point LIBS (volatile sodium), the proportion of atomic sodium in the total volatile sodium is given in Table 4. Almost 23% of the Na released is atomic sodium, which is in agreement with the CHEMKIN prediction (1892 K) on the sodium species in the flame at chemical equilibrium, as shown in Table 5. In our CHEMKIN simulations, the temperature and the main gas compositions of the plume were chosen to be the same as in the outlet of the heat-flux burner (see Section 2.1). Moreover, the released sodium, chlorine and sulfur were assumed to be atomic Na, HCl and SO_2 [22]. It should be noted that the equilibrium results are not affected by the initial chemical forms of Na [15]. The initial concentrations of atomic Na, HCl and SO_2 were estimated based on the mean burning rate of the coal particle and the species compositions in the chemical analyses shown in Table 1 and Table 2. Based on the CHEMKIN results, we can infer that atomic Na and NaOH are the two most favored species during coal

283 combustion. When the temperature increases from 1750 to 1950 K, the concentration of the two
284 major sodium compounds Na and NaOH change from 11.08% to 29.01% and from 87.31% to
285 69.97%, respectively. A simple sensitivity analysis can be calculated as follows:

$$\text{Sensitivity}=\frac{\text{Percentage change in target value}}{\text{Percentage change in parameter value}} \quad (13)$$

286 From 1800 K to 1900 K, the temperature has changed +5.6%, and the sensitivity of the
287 concentrations of Na and NaOH are 11.09 and -1.88, respectively, which indicates atomic sodium
288 can be quite sensitive to the temperature.

289 However, the proportion of atomic sodium in volatile Na is not constant during the
290 combustion of the coal particle, with a much higher proportion in the ash stage than in the
291 previous two combustion stages. As atomic sodium is produced by decomposition of Na
292 compounds in the region near the coal particle sample, the proportion of atomic sodium is
293 dependent on the particle temperature and parent compound. A higher temperature yields stronger
294 decomposition of Na compounds, thus a higher proportion of atomic sodium. However, in the ash
295 reaction stage the particle temperature is lower than in the char burning and de-volatilization
296 stages, so the high atomic Na in the ash reaction stage must be due to the Na compound released
297 during the ash stage having a higher decomposition rate than in the previous two stages.

298 **3.2 Particle temperature and diameter measurement**

299 The sodium concentration in the solid phase (Na_{solid}) can be determined by subtraction of
300 multi-point LIBS results (Fig. 5a) from the total sodium concentration (Table 2). The relationship
301 between combustion parameters, such as the particle diameter (d), the surface temperature (T), and
302 Na_{solid} of 4-mm particle combustion is shown in Fig. 6a. And their derivatives are shown in Fig. 6b.
303 The curves of d and T with time can be clearly divided into the three stages of the coal particle

304 combustion:

305 (I) As shown in Fig. 6a, at the beginning, the particle is suddenly put into the plume so T
306 increases to nearly 1500 K in several seconds. Then the particle starts to pyrolyze and the volatiles
307 will burn around the particle, accelerating the heating of the particle by thermal radiation. During
308 this period, r is almost constant but Na_{solid} decreases as long as the particle stays in the plume.
309 According to [21], a lot of water-soluble sodium will evaporate and transform in this period. After
310 the volatile components have burned out, both T and Na_{solid} experience an inflection point because
311 of the lack of thermal radiation from the burning of volatile components.

312 (II) The ignition and burning of char causes the decrease of the particle diameter, indicating
313 the combustion stage has moved to the second one. In this period, the char reacts with gas-phase
314 components, generating heat and shrinking the core of the particle. This reaction will promote the
315 temperature of the particle and then accelerate the reaction. So an increase of $\mathrm{d}d/\mathrm{d}t$ and $\mathrm{d}Na_{solid}/\mathrm{d}t$
316 can be observed (Fig. 6b). Both $\mathrm{d}d/\mathrm{d}t$ and $\mathrm{d}Na_{solid}/\mathrm{d}t$ reach their maximum magnitudes in this
317 period. Most of the organic sodium is released at this stage, due to the organic compounds being
318 destroyed by combustion.

319 (III) After the char burnout, the residues transform to a stable status. T and Na_{solid} are almost
320 constant and d shows a slight decrease with time (Fig. 6a). By analyzing the derivatives, there is
321 still some minor sodium release in this period. Previous research shows that the ash can react with
322 water vapor in the plume, causing the release of sodium [17].

323 The similar tendencies observed in the profiles of the sodium mass and the combustion
324 parameters reveal that the release of sodium components is related to the burning of the coal
325 particle. The variations of Na_{solid} and d with time are very similar, which implies Na_{solid} may have

326 a relationship with the particle volume (V). Moreover, dNa_{solid}/dt is very similar to T, which means
327 the sodium flux can be determined by the particle temperature.

328 We can deduce the correlations by plotting the particle volume and Na_{solid}. Fig. 7 shows their
329 correlation in the char burnout and ash reaction stages. In order to obtain general conclusions, the
330 6-mm-particle results, which are obtained by the same method as for the 4-mm particles, are also
331 shown in Fig. 7. The total fractional sodium release from the 6 mm particle is 38.4% due to the
332 larger particle size will lead to the release of sodium with a lower proportion. Both results of the
333 4-mm and 6-mm particles show a linear relationship between Na_{solid} and V. Using a linear fitting,
334 the correlation between Na_{solid} and V can be approximated by:

$$\begin{cases} 4\ mm\ Na_{solid} = 0.004882 \times V + 0.2167, R^2 = 0.9947 \\ 6\ mm\ Na_{solid} = 0.005194 \times V + 0.6878, R^2 = 0.9887 \end{cases} \tag{14}$$

335 where the units of Na_{solid} and V are mg and mm^3, respectively. According to [38], during the char
336 burnout stage the sodium compounds are most likely sodium carbonate and then released into the
337 gas phase by char combustion. Therefore the residual sodium mass in the coal particle, i.e., Na_{solid},
338 may be related to the mass of the particle during char combustion. Moreover, the mass of the
339 particle is reflected in its volume change, as shown in the shrinking core model [39]. In addition,
340 the combustion of the particle will destroy the particle structure and lead to the sodium which
341 storage in the porous to release. So a general relationship may exist between Na_{solid} and V. We
342 normalize Na_{solid} and V by their initial value for 4-mm and 6-mm particles, and the correlation is
343 plotted in Fig. 8.

$$\begin{cases} Na'_{solid} = \dfrac{Na_{solid}}{Na_{solid,initial}} \\ V' = \dfrac{V}{V_{initial}} \end{cases} \tag{15}$$

344 where the initial values used here are determined from those before the start of the burning. After

345 the normalization, the results of the particles in two different sizes overlap with each other. By
346 fitting the scatter results, the general correlation between Na_{solid} and V of a burning Zhundong coal
347 particle can be approximated by:

$$\frac{Na_{solid}}{Na_{solid,initial}} = \frac{V}{V_{initial}} \times 0.4406 + 0.5728, R^2 = 0.9829 \tag{16}$$

348 **3.3 Kinetics of sodium release**

349 The rate of sodium release can be obtained from the derivative of Na_{solid} with time. Since
350 Na_{solid} has a linear relationship with the particle volume, the sodium release rate should be based
351 on the combustion rate of the coal particle. In general, the coal particle combustion rate usually
352 obeys an Arrhenius expression. van Eyk et al. [17] has established a relationship between the rate
353 of sodium release and char temperature in the char burnout stage,

$$\begin{cases} Na_{flux,t} = Na_{solid} \times k \\ k = A \times \exp(-E/(R \times T)) \end{cases} \tag{17}$$

354 where k is the chemical rate constant for sodium release, A is the pre-exponential factor, E is
355 activation energy, and R is the universal gas constant, 8.314 J/(mol•K). They assumed that all the
356 sodium in the coal was releasable and the temperature distribution in the char particle is uniform.
357 In this study, it was found that only 47% of the total sodium could be released. So Eq. (17) has
358 been modified to:

$$\begin{cases} Na_{flux,t} = Na_{volatile,t} \times k \\ Na_{volatile,t} = \int_0^{\infty} Na_{flux,LIBS} \times dt - \int_0^{t} Na_{flux,LIBS} \times dt \\ k = A \times \exp(-E/(R \times T)) \end{cases} \tag{18}$$

359 where $Na_{volatile,t}$ means the mass of releasable sodium remaining in the particle and it is determined
360 from our LIBS experiments. In this case, we can determine k by using the experimental results:

$$k = \frac{Na_{flux,\mathrm{LIBS}}}{\int_0^{\infty} Na_{flux,\mathrm{LIBS}} \times dt - \int_0^{t} Na_{flux,\mathrm{LIBS}} \times dt} \tag{19}$$

361 The variation of k with time in the 4-mm particle experiments is shown in Fig. 9a. The curve
362 of k is similar to the sodium flux curve, but the appearance of the peaks is delayed compared to
363 those of $Na_{flux,t}$. After getting the values of k, A and E can be determined by the following
364 equation:

$$\ln(k) = \ln(A) - \frac{E}{R} \times \frac{1}{T} \tag{20}$$

365 Hence, by plotting ln(k) versus -1/T, we can calculate the values of A and E through the
366 interception and slope of the fitted line, respectively. In our study, we choose the char burnout
367 stage as the calculation zone and can get a linear correlation (Fig. 9b) as:

$$\ln(k) = 14.088 - 34624.98 / T, R^2 = 0.9798 \tag{21}$$

368 With Eq. (21), we can determine A and E, and the reaction rate k for sodium release as:

$$k = 10^{6.118} \times \exp(\frac{-287.8\,\text{kJ/ mol}}{R \times T}) \tag{22}$$

369 As discussed in our previous work [37], a coal particle undergoes the pyrolysis process at the
370 beginning of combustion. So the release of sodium can be strongly influenced by the pyrolysis of
371 the coal particle. In order to incorporate this effect, we have developed a two-step kinetics model
372 to separately account for the release of the two types of sodium (sodium compounds bounded to
373 volatile and char) when the coal particle is burning. In the previous work [37], a two-step model
374 has been developed to approximate the kinetics of atomic sodium release. The two-step model was
375 adapted in the present study to obtain the kinetics of volatile sodium (including NaOH, NaCl,
376 Na_2SO_4, Na etc.) release. We assumed that k_2 in Eq. (23) is equal to k in Eq. (22), and the two
377 types of volatile Na are calculated based on the chemical analyses in Table 1 and Table 2. The
378 equations of the two-step kinetics are:

$$\begin{cases} Na_{flux,t} = Na_{volatile,V,t} \times k_1 + Na_{volatile,C\&A,t} \times k_2 \\ Na_{volatile,V,t} = Na_{volatile,t} \times V_d \\ Na_{volatile,C\&A,t} = Na_{volatile,t} \times (FC_d + A_d) \\ k_1 = A_1 \times \exp(-E_1 / (R \times T)) \\ k_2 = A_2 \times \exp(-E_2 / (R \times T)) \end{cases} \quad (23)$$

where $Na_{volatile,V,t}$ is the volatile sodium bonded to the volatile matter and $Na_{volatile,C\&A,t}$ is the volatile sodium bonded to the char and ash. V_d, FC_d and A_d are the mass fractions of volatile matter, fixed carbon and ash in the coal by dry basis (Table 1). By recalculating the volatile sodium flux based on the two-step kinetics, the value of k_1 can be determined as:

$$k_1 = 10^{6.083} \times \exp(\frac{-279.3\ kJ\ /\ mol}{R \times T}) \quad (24)$$

Verification of the sodium release kinetics has been presented for coal particles of the two diameters: 4 mm and 6 mm. The input kinetics is Eqs. (22) and (24), and other parameters, such as T and initial sodium concentrations, are taken from our multi-point LIBS measurements. The comparisons between the experimental and simulation results are shown in Fig. 10. They agree well with each other for both the 4-mm and 6-mm particles. For sodium flux, both the one-step and two-step kinetics models predict a lower magnitude of the peaks both in the de-volatilization and char burnout stages than the experimental results. This also leads to the model predictions of Na_{solid} being higher than the experimental results. Compared to the one-step kinetics, the two-step kinetics agrees better with the experimental results, and it can successfully predict the sodium release during the whole course of the combustion of a single coal particle, including the initial devolatilization stage.

4 Conclusions

A multi-point LIBS method for quantitative measurement of sodium concentrations in the plume during the burning of a Zhundong coal particle has been presented. The particle surface temperature and particle diameter are measured simultaneously. In this study, 42.2 % of sodium

was released during the burning of a 4-mm Zhundong coal particle, which agrees well with both the offline chemical analysis in Table 2 (47.5%) and the mass balance of sodium (49.7%). The measurement of a 4-mm Zhundong coal particle shows in the char burnout stage, sodium release is the strongest (87% of the overall releasable sodium). The ratios of sodium released to the overall releasable sodium in the de-volatilization and ash reaction stages are 5% and 8%, respectively. The most favored species in the plume at chemical equilibrium are atomic Na and NaOH, based on CHEMKIN predictions.

A detailed analysis of the residual sodium mass, particle surface temperature and particle diameter suggests the sodium release is closely related to the particle burning status. The profile of the sodium release rate is very similar to the variation of the particle surface temperature. Moreover, the variation of the sodium mass in the residue has the same tendency as that of the particle diameter. A linear relationship between the sodium mass in the residue and the particle volume of a burning Zhundong coal particle is determined as:

$$Na_{solid} / Na_{solid,initial} = V / V_{initial} \times 0.4406 + 0.5728, R^2 = 0.9829 \quad .$$

The sodium release rate obeys an Arrhenius expression. The kinetics of sodium release during Zhundong coal combustion determined by a one-step model has the pre-exponential factor of $10^{6.11}$ s^{-1} and the activation energy of 287.8 kJ/mol. Moreover, a modified van Eyk's model, i.e. a two-step model that separately considers the influence of devolatilization and char burnout on sodium release, has been developed. The two-step kinetics model predictions agree well with the experimental results in the verification study, including the sodium release at the initial burning stage.

Acknowledgements

This work was supported by the National Natural Science Foundation of China (51422605, 51390491) and the Ph.D. Programs Foundation of Ministry of Education of China (20130101110095).

Reference

[1] M. Neville, A.F. Sarofim, The fate of sodium during pulverized coal combustion, Fuel 64 (1985) 384-390.

[2] H.P. Nielsen, F.J. Frandsen, K. Dam-Johansen, L.L. Baxter, The implications of chlorine-associated corrosion on the operation of biomass-fired boilers, Prog. Energy Combust. Sci. 26 (2000) 283-298.

[3] R.W. Bryers, Fireside slagging, fouling, and high-temperature corrosion of heat-transfer surface due to impurities in steam-raising fuels, Prog. Energy Combust. Sci. 22 (1996) 29-120.

[4] H. Zhou, B. Zhou, L. Li, H. Zhang, Experimental Measurement of the Effective Thermal Conductivity of Ash Deposit for High Sodium Coal (Zhun Dong Coal) in a 300 KW Test Furnace, Energy Fuels 27 (2013) 7008-7022.

[5] R.J. Quann, M. Neville, M. Janghorbani, C.A. Mims, A.F. Sarofim, Mineral matter and trace-element vaporization in a laboratory-pulverized coal combustion system, Environ. Sci. Technol. 16 (1982) 776-781.

[6] T. Takuwa, I. Naruse, Detailed kinetic and control of alkali metal compounds during coal combustion, Fuel Process. Technol. 88 (2007) 1029-1034.

[7] S.A. Benson, P.L. Holm, Comparison of inorganics in three low-rank coals, Ind. Eng. Chem. Res. 24 (1985) 145-149.

[8] J. Zhang, C.-L. Han, Z. Yan, K. Liu, Y. Xu, C.-D. Sheng, W.-P. Pan, The Varying Characterization of Alkali Metals (Na, K) from Coal during the Initial Stage of Coal Combustion, Energy Fuels 15 (2001) 786-793.

[9] Y. He, K. Qiu, R. Whiddon, Z. Wang, Y. Zhu, Y. Liu, Z. Li, K. Cen, Release characteristic of different classes of sodium during combustion of Zhun-Dong coal investigated by laser-induced breakdown spectroscopy, Sci. Bull. 60 (2015) 1927-1934.

[10] P. Monkhouse, On-line diagnostic methods for metal species in industrial process gas, Prog. Energy Combust. Sci. 28 (2002) 331-381.

[11] F. Greger, K.T. Hartinger, P.B. Monkhouse, J. Wolfrum, H. Baumann, B. Bonn, In situ alkali concentration measurements in a pressuried, fluidized-bed coal combustor by excimer laser induced fragmentation fluorescence, Symposium (International) on Combustion 26 (1996) 3301-3307.

[12] E. Schlosser, T. Fernholz, H. Teichert, V. Ebert, In situ detection of potassium atoms in high-temperature coal-combustion systems using near-infrared-diode lasers, Spectroc. Acta Pt. A-Molec. 58 (2002) 2347-2359.

[13] Y. He, J. Zhu, B. Li, Z. Wang, Z. Li, M. Aldén, K. Cen, In-situ Measurement of Sodium and Potassium Release during Oxy-Fuel Combustion of Lignite using Laser-Induced Breakdown Spectroscopy: Effects of O2 and CO2 Concentration, Energy Fuels 27 (2013) 1123-1130.

[14] P.J. van Eyk, P.J. Ashman, Z.T. Alwahabi, G.J. Nathan, Quantitative measurement of atomic sodium in the plume of a single burning coal particle, Combust. Flame 155 (2008) 529-537.

[15] P.J. van Eyk, P.J. Ashman, Z.T. Alwahabi, G.J. Nathan, The release of water-bound and organic sodium from Loy Yang coal during the combustion of single particles in a flat flame, Combust. Flame 158 (2011) 1181-1192.

[16] S. Akbar, U. Schnell, G. Scheffknecht, Modelling potassium release and the effect of potassium chloride on deposition mechanisms for coal and biomass-fired boilers, Combust. Theory Model. 14 (2010) 315-329.
[17] P.J. van Eyk, P.J. Ashman, G.J. Nathan, Mechanism and kinetics of sodium release from brown coal char particles during combustion, Combust. Flame 158 (2011) 2512-2523.
[18] M.U. Garba, D.B. Ingham, L. Ma, R.T.J. Porter, M. Pourkashnian, H.Z. Tan, A. Williams, Prediction of Potassium Chloride Sulfation and Its Effect on Deposition in Biomass-Fired Boilers, Energy Fuels 26 (2012) 6501-6508.
[19] J.G. Olsson, U. Jäglid, J.B.C. Pettersson, P. Hald, Alkali Metal Emission during Pyrolysis of Biomass, Energy Fuels 11 (1997) 779-784.
[20] K. Yase, Y. Takahashi, N. Ara-Kato, A. Kawazu, Evaporation rate and saturated vapor pressure of functional organic materials, Jpn. J. Appl. Phys. 34 (1995) 636.
[21] J. Tomeczek, K. Wacławiak, Two-dimensional modelling of deposits formation on platen superheaters in pulverized coal boilers, Fuel 88 (2009) 1466-1471.
[22] A. Kosminski, D.P. Ross, J.B. Agnew, Transformations of sodium during gasification of low-rank coal, Fuel Process. Technol. 87 (2006) 943-952.
[23] S.C. van Lith, P.A. Jensen, F.J. Frandsen, P. Glarborg, Release to the gas phase of inorganic elements during wood combustion. Part 2: influence of fuel composition, Energy Fuels 22 (2008) 1598-1609.
[24] I.L.C. Freriks, H.M.H. van Wechem, J.C.M. Stuiver, R. Bouwman, Potassium-catalysed gasification of carbon with steam: a temperature-programmed desorption and Fourier Transform infrared study, Fuel 60 (1981) 463-470.
[25] C.A. Mims, J.K. Pabst, Fundamentals of Catalytic Coal and Carbon GasificationRole of surface salt complexes in alkali-catalysed carbon gasification, Fuel 62 (1983) 176-179.
[26] F. Shadman, D.A. Sams, W.A. Punjak, Significance of the reduction of alkali carbonates in catalytic carbon gasification, Fuel 66 (1987) 1658-1663.
[27] W.B. Weng, Z.H. Wang, Y. He, R. Whiddon, Y.J. Zhou, Z.S. Li, K.F. Cen, Effect of N2/CO2 dilution on laminar burning velocity of H2–CO–O2 oxy-fuel premixed flame, Int. J. Hydrog. Energy 40 (2015) 1203-1211.
[28] L.-J. Hsu, Z.T. Alwahabi, G.J. Nathan, Y. Li, Z.S. Li, M. Aldén, Sodium and Potassium Released from Burning Particles of Brown Coal and Pine Wood in a Laminar Premixed Methane Flame Using Quantitative Laser-Induced Breakdown Spectroscopy, Appl. Spectroc. 65 (2011) 684-691.
[29] R. Khatami, Y.A. Levendis, On the deduction of single coal particle combustion temperature from three-color optical pyrometry, Combust. Flame 158 (2011) 1822-1836.
[30] B. Müller, U. Renz, Development of a fast fiber-optic two-color pyrometer for the temperature measurement of surfaces with varying emissivities, Rev. Sci. Instrum. 72 (2001) 3366-3374.
[31] Y. Huang, Y. Yan, G. Riley, Vision-based measurement of temperature distribution in a 500-kW model furnace using the two-colour method, Measurement 28 (2000) 175-183.
[32] D.P. DeWitt, G.D. Nutter, Theory and practice of radiation thermometry, Wiley Online Library1988.
[33] P.J. van Eyk, P.J. Ashman, Z.T. Alwahabi, G.J. Nathan, Simultaneous measurements of the release of atomic sodium, particle diameter and particle temperature for a single burning coal particle, Proc. Combust. Inst. 32 (2009) 2099-2106.
[34] J. Zhou, X. Zhuang, A. Alastuey, X. Querol, J. Li, Geochemistry and mineralogy of coal in the

recently explored Zhundong large coal field in the Junggar basin, Xinjiang province, China, Int. J. Coal Geol. 82 (2010) 51-67.
[35] Z. Wang, Y. Liu, Y. He, R. Whiddon, K. Wan, J. Xia, J. Liu, Effects of Microwave Irradiation on Combustion and Sodium Release Characteristics of Zhundong Lignite, Energy Fuels 30 (2016) 8977-8984.
[36] H. Fatehi, Y. He, Z. Wang, Z.S. Li, X.S. Bai, M. Aldén, K.F. Cen, LIBS measurements and numerical studies of potassium release during biomass gasification, Proc. Combust. Inst. 35 (2015) 2389-2396.
[37] Z. Wang, Y. Liu, R. Whiddon, K. Wan, Y. He, J. Xia, K. Cen, Measurement of atomic sodium release during pyrolysis and combustion of sodium-enriched Zhundong coal pellet, Combust. Flame 176 (2017) 429-438.
[38] E. Lindner, A study of sodiumash reactions during the pulverised coal combustion, PhD thesis, Department of Chemical Engineering, University of Newcastle, Australia, 1988.
[39] A.K. Sadhukhan, P. Gupta, R.K. Saha, Modelling of combustion characteristics of high ash coal char particles at high pressure: Shrinking reactive core model, Fuel 89 (2010) 162-169.

525 **Table 1.** Chemical analysis of Zhundong coal

Proximate analysis(wt.%, air dry basis)				
Moisture	Ash	Volatile	Fix Carbon	
9.85	4.23	28.72	57.2	
Ultimate analysis(wt.%, dry ash free basis)				
Carbon	Hydrogen	Nitrogen	Sulfur	Oxygen
79.29	2.89	0.88	0.43	16.5
Cl (mg/g coal, air dry basis)				
2.56				

526
527
528
529
530
531 **Table 2.** Mass (mg) of different classes of sodium in a 1g coal particle

Sample	Na mass (mg/1 g of raw coal)				
	Water-soluble	NH_4Ac-soluble	HCl-soluble	Insoluble	Total
Raw coal	4.946	0.55	0.334	1.579	7.409
Ash	1.894	0.095	0.31	1.593	3.892
Released Na mass	3.052	0.455	0.024	0	3.517
Relative Released Proportion (= released Na mass / total Na mass in raw coal)	61.70%	82.70%	7.18%	0	47.5%

532
533
534
535
536
537 **Table 3.** Fitting coefficients

	a_2	a_1	a_0	R^2
$f_{30s}(r)$	-0.00253	-0.4608	6.502	0.9801
$f_{400s}(r)$	0.01629	-1.289	13.78	0.9868
$f_{800s}(r)$	0.003176	-0.08052	0.5356	0.9895

	b_4	b_3	b_2	b_1	b_0	R^2
$f_{tt}(r)$	8.104E-06	-0.00028	0.002113	0.001174	0.1442	0.9986

538
539
540
541
542

Table 4. Sodium release in different coal-burning stages (unit: mg/50 mg of raw coal)

	devolatilization	char burning	ash reaction	total
Atomic sodium	1.519E-3	3.030E-2	5.729E-3	0.037
Volatile sodium	0.008	0.136	0.013	0.156
Proportion of atomic sodium %	18.9%	22.3%	44.1%	24%

Table 5. Equilibrium compositions of sodium compounds in the plume at 1750~1950 K predicted by CHEMKIN.

Temperature	Different sodium proportion (%)				
	Na	NaO	NaO_2	NaOH	NaCl
1750	11.08	0.25	0.09	87.31	1.31
1800	14.69	0.32	0.09	83.99	0.94
1850	18.93	0.40	0.08	79.92	0.67
1892	22.94	0.47	0.08	76.00	0.51
1900	23.74	0.49	0.08	75.20	0.48
1950	29.01	0.58	0.08	69.97	0.35

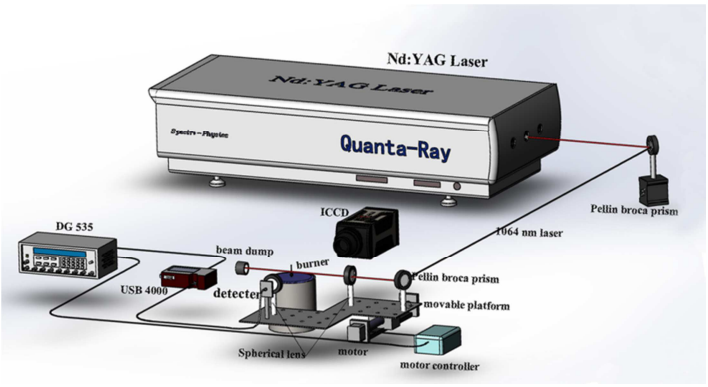

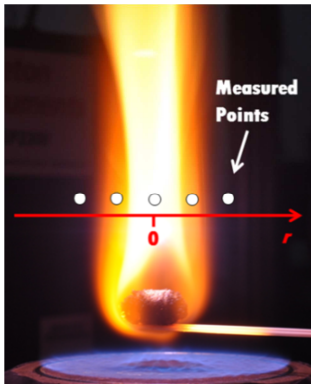

(a) Configuration (b) LIBS measurment points

Fig. 1. Multi-point LIBS experiment setup.

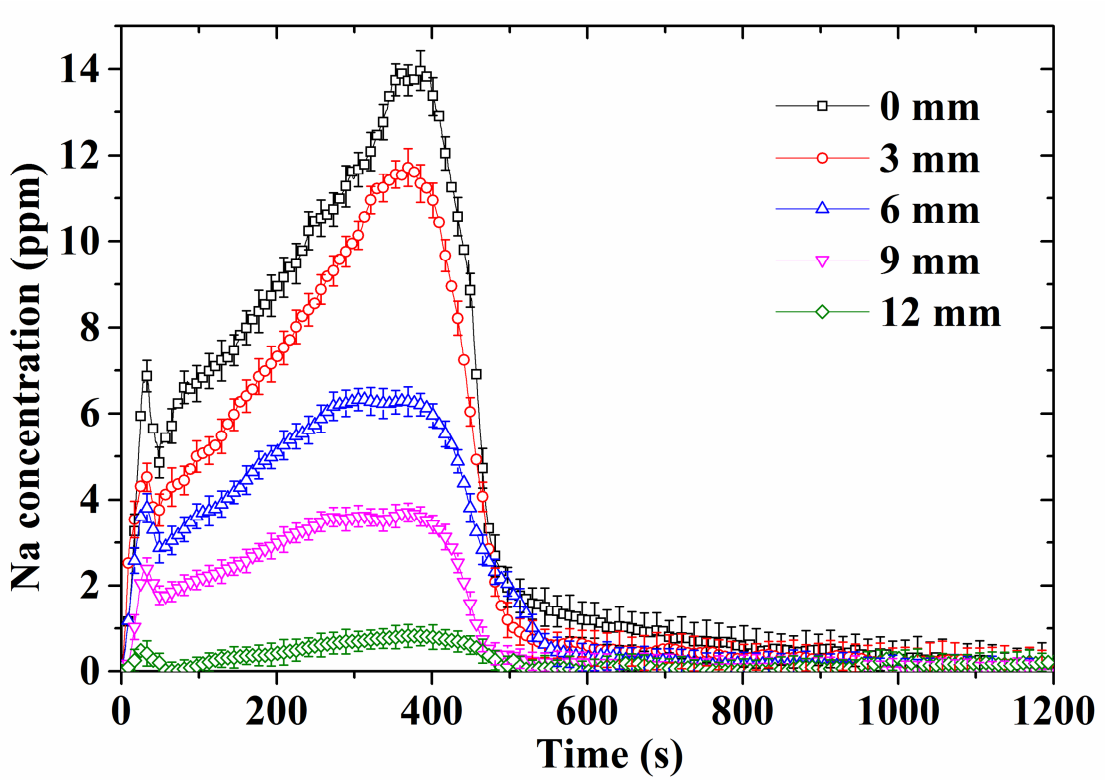

Fig. 2. LIBS data of sodium element concentrations at different measurement points (r = 0, 3, 6, 9, 12 mm) during the combustion of a 4-mm coal particle. (the concentration at 15 mm is always below the detected limit of 0.3 ppm)

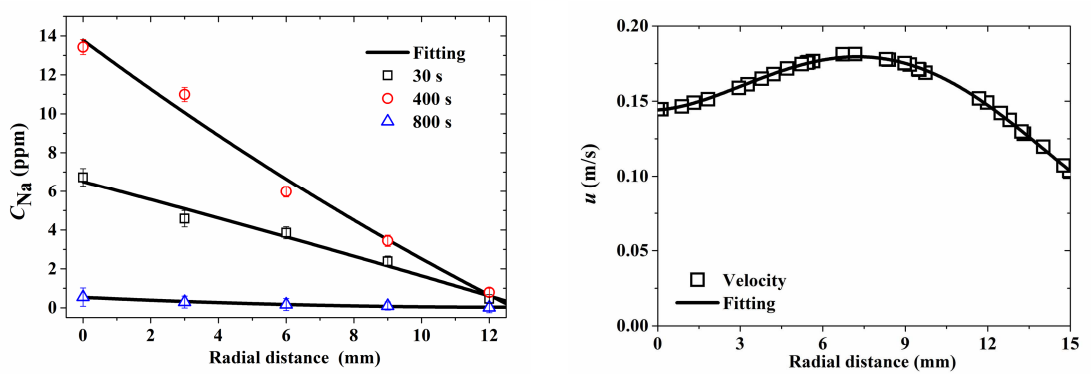

(a) Sodium concentration distribution (b) Axial velocity distribution

Fig. 3. Profiles of sodium concentration and axial velocity distributions along the radial direction at 10mm above the 4-mm Zhundong coal particle.

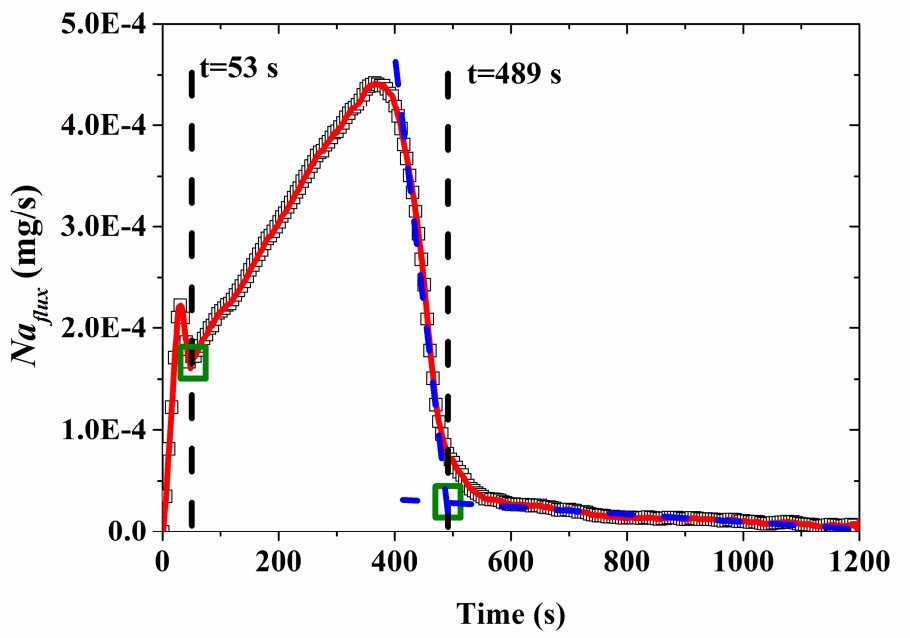

569

570 **Fig. 4** The determination of three sodium release stages.

571

572

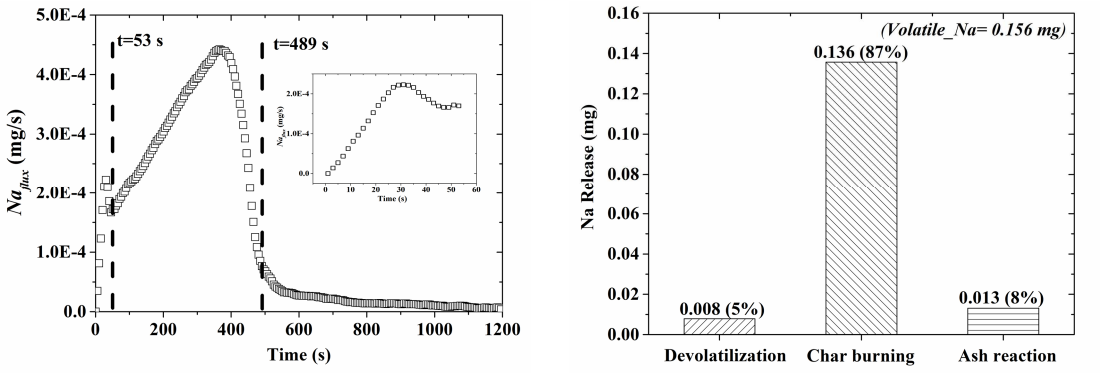

(a) sodium flux (b) Na release proportion in different stages

Fig. 5. Profile of sodium flux and statics of Na release in different coal-burning stages (4-mm particle).

577

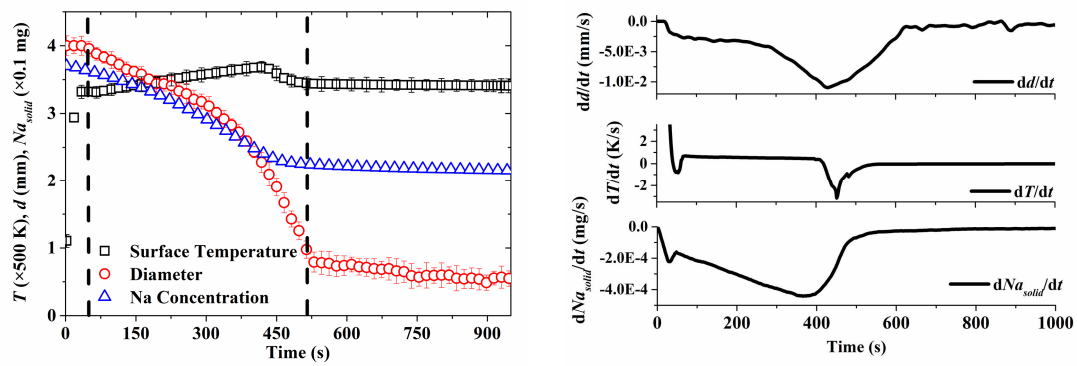

(a) T, d and Na_{solid} (b) dT/dt, dd/dt and dNa_{solid}/dt

578 **Fig. 6.** Variation and derivatives of particle surface temperature (T), particle diameter (d) and
579 sodium mass in the solid phase (Na_{solid}) with time (4mm particle).

580

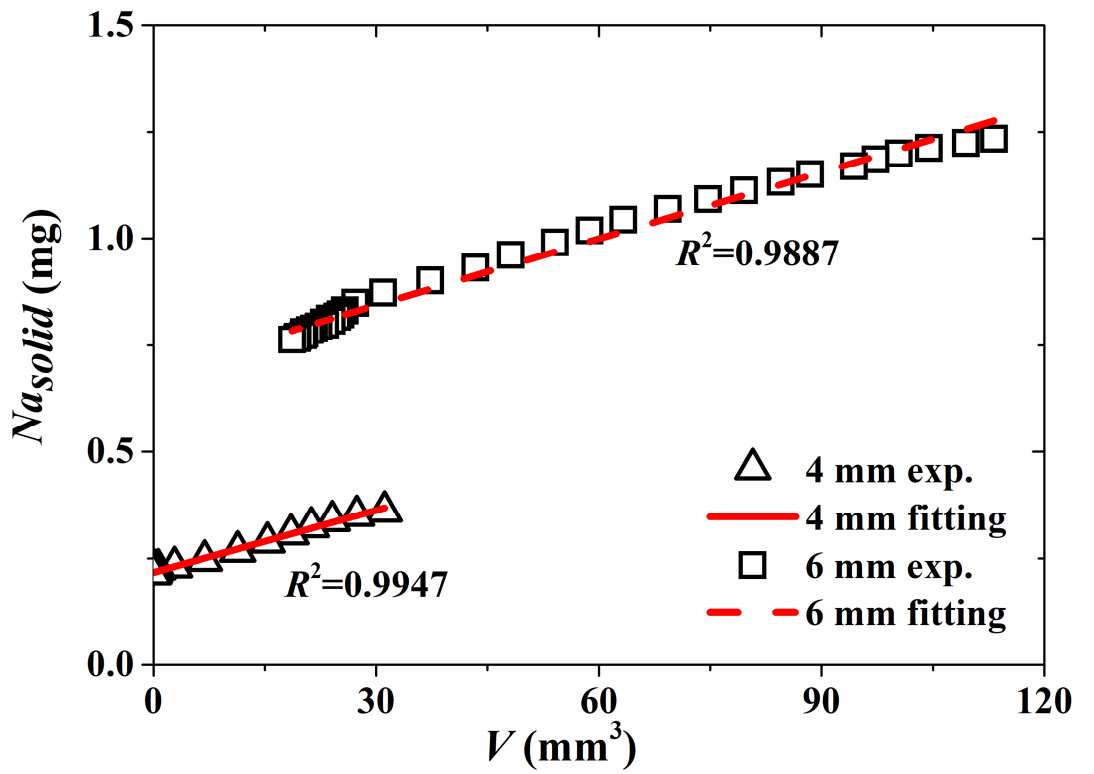

581

582 **Fig. 7.** The relationship between sodium mass in the solid phase (Na_{solid}) and particle volume (V)

583

584

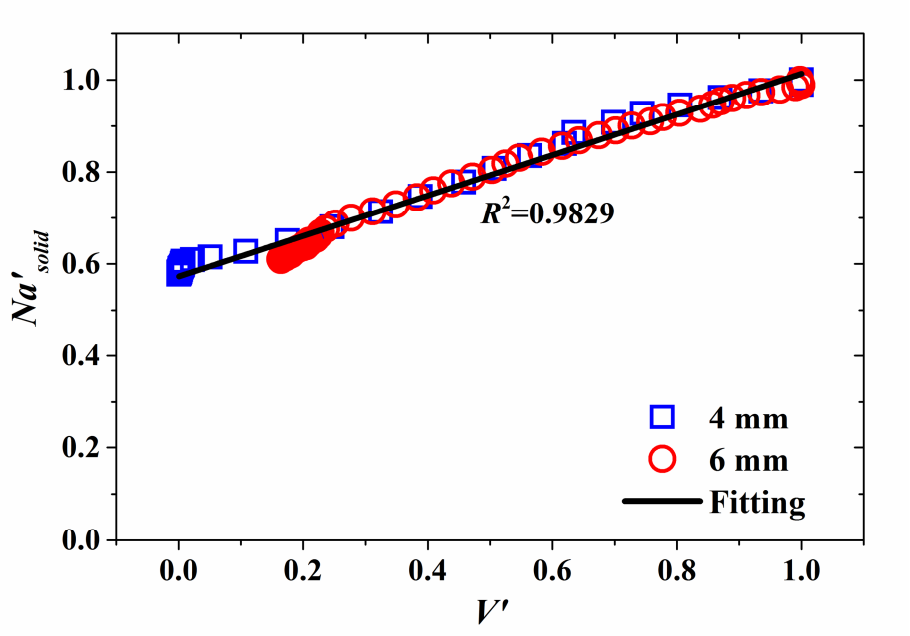

585

586 **Fig. 8.** The correlation between normalized solid-phase sodium mass (Na'_{solid}) and normalized
587 particle volume (V')

588

589

590

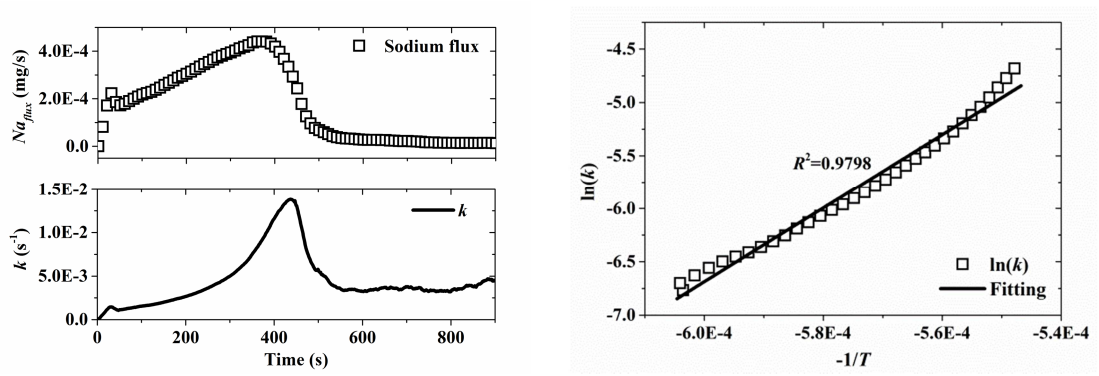

(a) k (b) ln(k) versus -1/T

591 **Fig. 9.** Measurement results and kinetics model development, 4 mm Zhundong coal particle.

592

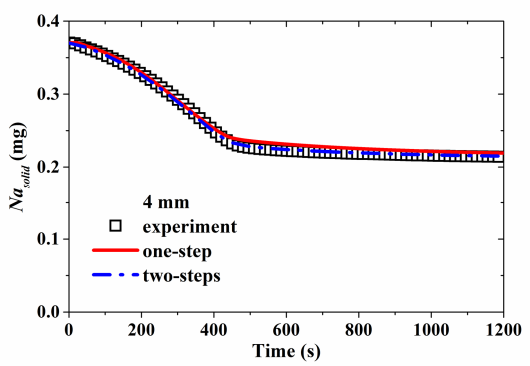

(a) 4-mm, Na concentration in the solid phase

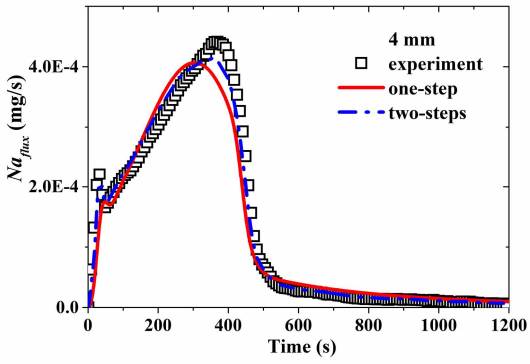

(b) 4-mm, sodium flux

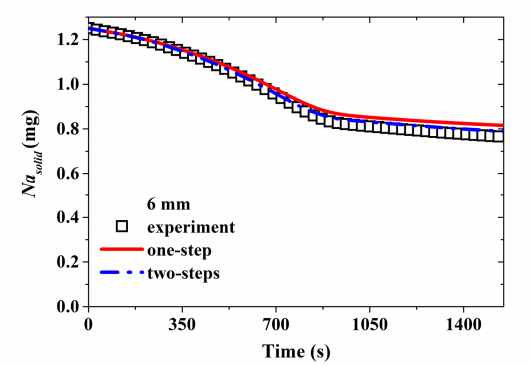

(c) 6-mm, Na concentration in the solid phase

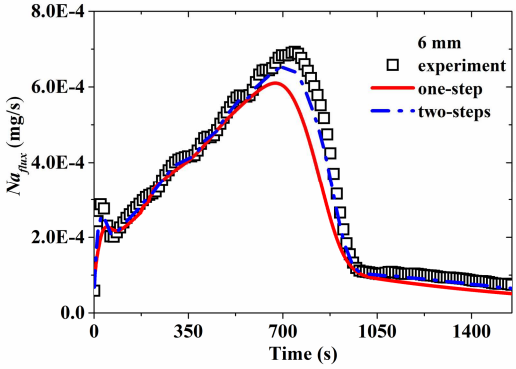

(d) 6-mm, sodium flux

Fig. 10. Verification of sodium release kinetics against measurement results.